Structure, Vol. 12, 1901–1907, October, 2004, ©2004 Elsevier Ltd. All rights reserved. DOI 10.1016/j.str.2004.08.003

The Crystal Structure of the Reduced, Zn^{2+}-Bound Form of the *B. subtilis* Hsp33 Chaperone and Its Implications for the Activation Mechanism

Izabela Janda,[1] Yancho Devedjiev,[1] Urszula Derewenda,[1] Zbigniew Dauter,[2] Jakub Bielnicki,[1] David R. Cooper,[1] Paul C.F. Graf,[3] Andrzej Joachimiak,[4] Ursula Jakob,[3] and Zygmunt S. Derewenda[1,*]

[1]Department of Molecular Physiology and Biological Physics
University of Virginia
Charlottesville, Virginia 22908

[2]Synchrotron Radiation Research Section
Macromolecular Crystallography Laboratory
NCI
Brookhaven National Laboratory
Upton, New York 11973

[3]Department of Molecular, Cellular and Developmental Biology
University of Michigan
Ann Arbor, Michigan 48109

[4]Biosciences Division and Structural Biology Center
Argonne National Laboratory
9700 South Cass Avenue
Building 202
Argonne, Illinois 60439

Summary

The bacterial heat shock protein Hsp33 is a redox-regulated chaperone activated by oxidative stress. In response to oxidation, four cysteines within a Zn^{2+} binding C-terminal domain form two disulfide bonds with concomitant release of the metal. This leads to the formation of the biologically active Hsp33 dimer. The crystal structure of the N-terminal domain of the *E. coli* protein has been reported, but neither the structure of the Zn^{2+} binding motif nor the nature of its regulatory interaction with the rest of the protein are known. Here we report the crystal structure of the full-length *B. subtilis* Hsp33 in the reduced form. The structure of the N-terminal, dimerization domain is similar to that of the *E. coli* protein, although there is no domain swapping. The Zn^{2+} binding domain is clearly resolved showing the details of the tetrahedral coordination of Zn^{2+} by four thiolates. We propose a structure-based activation pathway for Hsp33.

Introduction

Hsp33 is a novel bacterial molecular chaperone regulated by the redox conditions of the environment (Jakob et al., 1999). The *E. coli Hsp33* gene, well conserved and ubiquitous among prokaryotic organisms (Jakob et al., 1999; Korber et al., 1999), is found in an operon immediately downstream of the one encoding the Hsp15 heat shock protein. The amino acid sequence of the C-terminal domain of Hsp33 contains four absolutely conserved cysteines, Cys232, Cys234, Cys265, and Cys268 (*E. coli* numbering). They are found in a Cys-Xaa-Cys motif, followed by an approximately 30 residue long fragment, and a Cys-$(Xaa)_2$-Cys motif. This constitutes a novel type of a Zn^{2+} binding domain and is thought to directly regulate the activity of the Hsp33 protein (Jakob et al., 2000). Under normal conditions, Zn^{2+} is bound with very high affinity ($K_a > 10^{17}$ M^{-1}) by the thiolate moieties of the four cysteines (Jakob et al., 2000). Oxidative stress results in the release of zinc and the formation of two disulfides linking Cys232 with Cys234 and Cys265 with Cys268 (Barbirz et al., 2000), leading to significant conformational changes and concomitant dimerization of the protein (Graumann et al., 2001). Two recent independent crystallographic studies revealed the structure of the larger, N-terminal domain of the *E. coli* Hsp33, albeit in both cases the protein was C terminally truncated, so that residues beyond 233—corresponding to the entire Zn^{2+} binding domain—were not observed (Kim et al., 2001; Vijayalakshmi et al., 2001). Both structures revealed a tightly associated dimer formed by a domain crossover, so that an all helical fragment containing residues 179–218 from one monomer is packed onto the "back" of the N-terminal α/β type core of the other monomer. While both structures yielded significant insight into the overall Hsp33 architecture and dimerization mode, neither shed light on the mechanism of the activation switch leading to dimerization or on the mode of Zn^{2+} binding. Recently, biochemical and NMR studies suggested that under oxidizing conditions the C-terminal Zn^{2+} binding motif of Hsp33 undergoes essentially complete unfolding from a highly compact and predominantly helical structure (Graf et al., 2004). This oxidation-induced unfolding of Hsp33's redox switch domain appears to be crucial for the unmasking of the substrate binding site and dimerization interface, raising the possibility that the folded, reduced Zn^{2+} binding domain may interfere with substrate binding or dimerization. Once oxidized and dimerized, Hsp33 is highly active as a molecular chaperone and protects unfolded proteins against irreversible aggregation (Graf and Jakob, 2002). Upon return to reducing nonstress conditions, a kinetically stable, reduced Hsp33 dimer surprisingly retains its high affinity for substrate proteins. Release of the substrate proteins is triggered by the DnaK/DnaJ/GrpE chaperone machinery, which takes over the substrate proteins from the reduced Hsp33 dimers and supports their refolding to the native state. In the final step of the cycle, the substrate-free reduced Hsp33 dimers dissociate slowly into the biologically inactive, monomeric state (Hoffmann et al., 2004).

The full-length *B. subtilis* Hsp33 ortholog was originally selected as one of the targets by the Midwest Center for Structural Genomics (http://www.mcsg.anl.gov). However, the protein did not crystallize in the high-throughput pipeline. We have therefore used crystal engineering based on the concept of surface entropy reduction (Derewenda, 2004) to generate a crystallizable variant. A double mutant of the full-length protein, in

*Correspondence: zsd4n@virginia.edu

Table 1. Data Collection and Refinement Statistics

Data Collection Statistics		
	Peak (λ=1.2831 Å)	Inflection Point (λ = 1.2837 Å)
Space group and unit cell (Å)	$P3_121a = b = 115.3\ c = 106.4$	
Resolution (Å)[a]	50.0–1.97 (2.05–1.97)	30.0–1.97 (2.05–1.97)
Total reflections	460,699	543,743
Unique reflections	124,827 (12,464)	124,854 (12,466)
Redundancy	3.7 (3.7)	4.4 (4.3)
Completeness (%)[a]	100 (100)	100 (100)
R_{sym}[a,b] (%)	5.0 (51.2)	4.2 (35.2)
I/σ (I)[a,b]	24.57 (2.64)	34.7 (4.1)
Phasing Statistics		
Resolution (Å)	50.0–2.50	
Anomalous phasing power acentric[c]	0.34	
Anomalous R_{cullis}[d]	0.81	
Figure of merit	0.28	
Refinement Statistics		
Resolution (Å)	20.0–1.97	
Reflections (working)	56,615	
Reflections (test)	1,186	
R_{work} (%)[e]	19.7	
R_{free} (%)[e]	22.4	
Number of protein atoms	4,382	
Number of waters	277	
Number of acetate ions	6	
Number of Zn ions	2	
Rms deviations		
Bond lengths (Å)	0.025	
Bond angles (°)	1.849	
Average B factor (Å^2)		
Main chain	36.0	
Side chain	40.6	
Waters	39.2	

[a] Values in parentheses correspond to the last shell.
[b] $R_{sym} = \Sigma|I_i - \langle I\rangle|/\Sigma I$, where I_i is the intensity of the i-th observation, and $\langle I\rangle$ is the mean intensity of the reflections. The values are for unmerged Friedel pairs.
[c] Phasing power = rms ($|F_h|/E$), where $|F_h|$ is the heavy atom structure factor amplitude, and E is residual lack of closure error.
[d] $R_{cullis} = \Sigma||F_{h.obs}| - |F_{h.calc}||/\Sigma|F_h|$ for acentric reflections, where $|F_{h.obs}|$ is the observed heavy atom structure factor amplitude, and $|F_{h.calc}|$ is the calculated heavy atom structure factor amplitude.
[e] $R_{work} = \Sigma||F_{obs}| - |F_{calc}||/\Sigma|F_{obs}|$, crystallographic R factor, and $R_{free} = \Sigma||F_{obs}| - |F_{calc}||/\Sigma|F_{obs}|$, where all reflections belong to a test set of randomly selected data.

which alanines replaced the solvent-accessible Glu100 and Gln101, crystallized readily, and the resulting crystals yielded diffraction to 2.0 Å resolution. The refined crystal structure reveals a fully folded C-terminal Zn^{2+} binding motif, with the metal ion coordinated tetrahedrally by the thiolate groups of Cys235, Cys237, Cys268, and Cys271. Surprisingly, the N-terminal domains of two crystallographically independent molecules mediate the formation of a dimer closely reminiscent of the one observed for the *E. coli* protein, although no domain swapping is observed. We propose a general scheme for the reversible activation of Hsp33, triggered by the formation of intramolecular disulfides and sustained by the rate-limiting step of domain swapping.

Results and Discussion

Structure Solution and Quality of the Model

Given that the wild-type protein failed to crystallize, we applied the strategy of mutational surface entropy reduction to create patches conducive to crystal contact formation (Derewenda, 2004). Although this approach implies a screening process using several mutants, in the case of the *B. subtilis* Hsp33 (BsHsp33), only one mutant—in which residues Glu100 and Gln101 were replaced with alanines—was sufficient to yield X-ray quality crystals. The structure was solved using anomalous scattering from the Zn^{2+} ions and was refined at 2.00 Å resolution to a conventional crystallographic R factor of 19.7% and an R_{free} of 22.5% (Table 1). The asymmetric unit contains a dimer of BsHsp33 molecules, one Zn^{2+} ion bound per monomer, and a total of 6 acetate molecules and 277 water molecules. Although the crystals were soaked in 50 mM Zn acetate to ensure full Zn^{2+} occupancy, subsequent experiments revealed that this was not necessary (data not shown). The quaternary structure of the dimer is equivalent to that described for the N-terminal fragment of the *E. coli* protein (EcHsp33) (Kim et al., 2001; Vijayalakshmi et al., 2001). The packing in the crystal lattice is such that monomer A mediates most crystal contacts, while monomer B is involved primarily in intramolecular contacts. Consequently, mono-

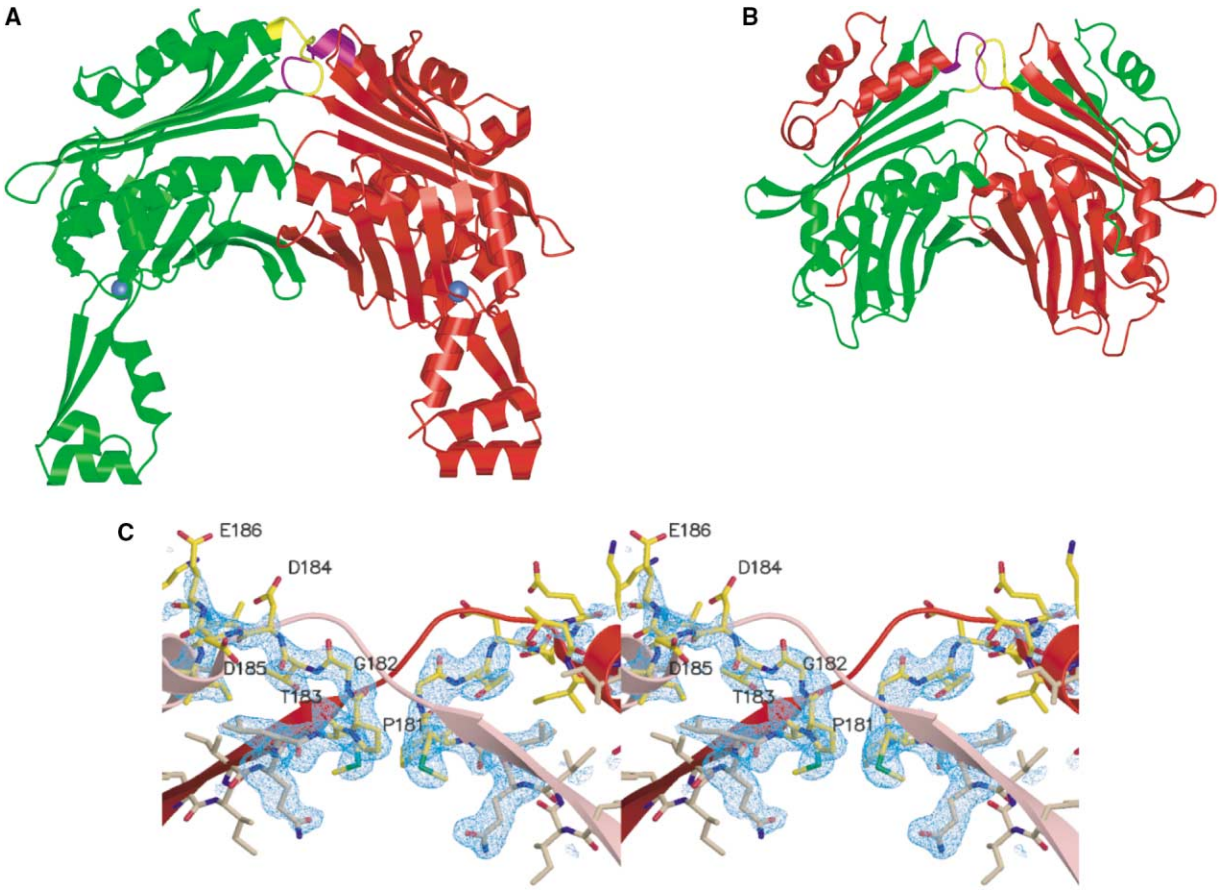

Figure 1. The Structure of Hsp33

(A) A ribbons representation of the *B. subtilis* Hsp33 noncrystallographic dimer. The two monomers are colored green and red, respectively. Yellow and magenta denote linker regions corresponding to those responsible in the *E. coli* protein for the domain-swapping effect. The zinc ions are shown as blue spheres. (B) The *E. coli* Hsp33 core domain, showing the architecture of domain swapping. The color code is the same as in (A).

(C) Stereo view of the omit electron density map contoured at 2.5 σ corresponding to the linker regions. The ribbon diagram shows the crossover as observed in the *E. coli* protein.

mer A has a lower mean main-chain temperature factor (32 Å^2) compared to monomer B (36 Å^2). There are 9 disordered residues in molecule A and 22 in molecule B. An analysis of the Ramachandran plot shows that 99.3% of the residues are in the most favored or allowed regions.

The *B. subtilis* and *E. coli* Hsp33 Proteins Have Similar Core Domains

The 24% amino acid sequence identity shared by the *B. subtilis* and *E. coli* proteins is consistent with a high level of structural similarity between the dimerization domains of the two proteins (Figures 1A and 1B). However, the reduced form of the BsHsp33 shows no domain swapping, which is well documented in the two reported structures of the EcHsp33 fragments (Kim et al., 2001; Vijayalakshmi et al., 2001). Residues 181–187, equivalent to the extended linker connecting the two swapped domains in the EcHsp33 structure (residues 178–184), show well-resolved electron density in both molecule A and B. They indicate how the fragment containing helices H5, H6, and H7, as defined in the EcHsp33 structures (Kim et al., 2001; Vijayalakshmi et al., 2001), folds back onto its parent molecule (Figure 1C). The helical domain (H5–H7) shows considerable intrinsic flexibility, as inferred from the conformational differences between the two molecules in the asymmetric unit. Among the most dramatic differences, the Pro181-Gly182 peptide is flipped in molecule A compared to B, and the oligopeptide Asp184-Thr187 forms a β turn in one case while it is an integral part of the H5 helix in the other.

Structure of the Zn^{2+} Binding Domain

The C-terminal, Zn^{2+} binding domain of the BsHsp33 adopts a unique tertiary fold with a significant helical content, as predicted by the CD and NMR spectroscopy (Graf et al., 2004). It consists of two short canonical loops (Harding, 2004) containing Cys235-Xaa-Cys237 and Cys268-$(Xaa)_2$-Cys271, which are connected by a 31-residue-long oligopeptide. Following the terminal β11 strand of the core domain (Vijayalakshmi et al., 2001), the polypeptide enters the Zn^{2+} binding domain in an extended conformation and then forms two short α helices (residues 239–250 and 251–263), an antiparallel

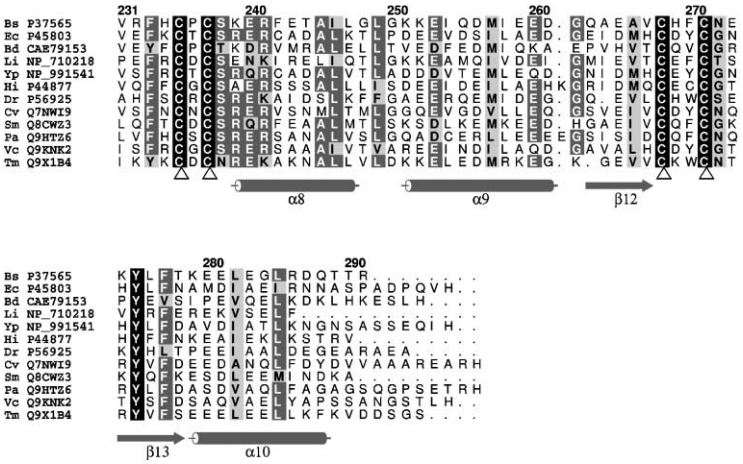

Figure 2. Sequence Homology of the C-Terminal Domain of Hsp33

The C-terminal domain of Hsp33 has been aligned using CLUSTALW. The zinc coordinating cysteines are indicated with arrows. The secondary structure of *Bacillus* protein is shown below the alignment. GenBank accession numbers are indicated on the left. Bs, *Bacillus subtilis*; Ec, *Escherichia coli*; Bd, *Bdellovibrio bacteriovorus*; Li, *Leptospira interrogans*; Yp, *Yersinia pestis*; Hi, *Haemophilus influenzae*; Dr, *Deinococcus radiodurans*; Cv, *Chromobacterium violaceum*; Sm, *Streptococcus mutans*; Pa, *Pseudomonas aeruginosa*; Vc, *Vibrio cholerae*; Tm, *Thermotoga maritim*.

hairpin β structure (residues 263–269 and 271–278), and a final α helix (residues 279–289) (Figure 1A). The tertiary fold brings together the hairpin and the initial extended stretch by means of the Zn^{2+} binding site and a small hydrophobic core of highly conserved Ile246, Ile254, Phe277, Leu282, and Leu285 (Figure 2). The Zn^{2+} ion is coordinated in a tetrahedral fashion by the thiolates of the four conserved cysteines. Cys235 and Cys237 are located at the N terminus of the domain, while Cys268 and Cys271 are located at the hairpin apex between two β strands (Figure 3). A comparison to other recently cataloged CCCC-type zinc binding proteins (Harding, 2004) revealed no structurally analogous examples, although, taken individually, short cysteine-containing loops are ubiquitous. The S-Zn^{2+} distances in BsHsp33 range from 2.27 Å to 2.39 Å, all within an experimental error of the expected 2.31 Å for a thiolate-Zn^{2+} bond (Simonson and Calimet, 2002). All four thiolates are involved in a network of H bonds which constitute the outer coordination sphere, similar to that described for the LIM2 domain of CRP2 (Konrat et al., 1998). Three of the thiolates (Cys235, Cys268, and Cys271) serve as H-bond acceptors for the main chain amides of Cys237, Phe270, and Glu273, respectively. The donor-acceptor distances range between 3.5 Å and 3.7 Å, well within the expected range. In addition, Cys235 also accepts an H bond from the Nη1 of Arg86 (3.4 Å), while Cys237, which has no amide proton donors in its vicinity, accepts an H bond from the hydroxyl of Tyr275. Arg86 is highly conserved (only two sequences show Lys in its place), while Tyr275 is the only absolutely conserved amino acid in the Zn^{2+} binding domain (except for the four cysteines) among the known Hsp33 homologs, suggesting an important structural and functional role. Interactions of arginines and tyrosines with thiolates are known in other redox-regulated proteins. For example, in the hydroperoxide resistance protein Ohr, the active site cysteine Cys60, which is directly involved in the peroxide reduction, in a ground state accepts a hydrogen bond from Nη1 of Arg18, also at 3.4 Å (Lesniak et al., 2002). In the isoenzyme 3-3 of glutathione S-transferase, the H bond between Tyr6 and the thiolate of the glutathione stabilizes the thiolate ion by 1.4–2.2 kcal/mol (Liu et al., 1992). Overall, this intricate H-bonding network is likely to substantially reduce the pK_a for the thiol groups, thus rationalizing the observed high affinity of this motif toward a Zn ion.

Mutual Disposition of the Zn^{2+} Binding and Dimerization Domains

The Zn^{2+} binding domain forms a very limited interface with the dimerization domain in BsHsp33, so that the

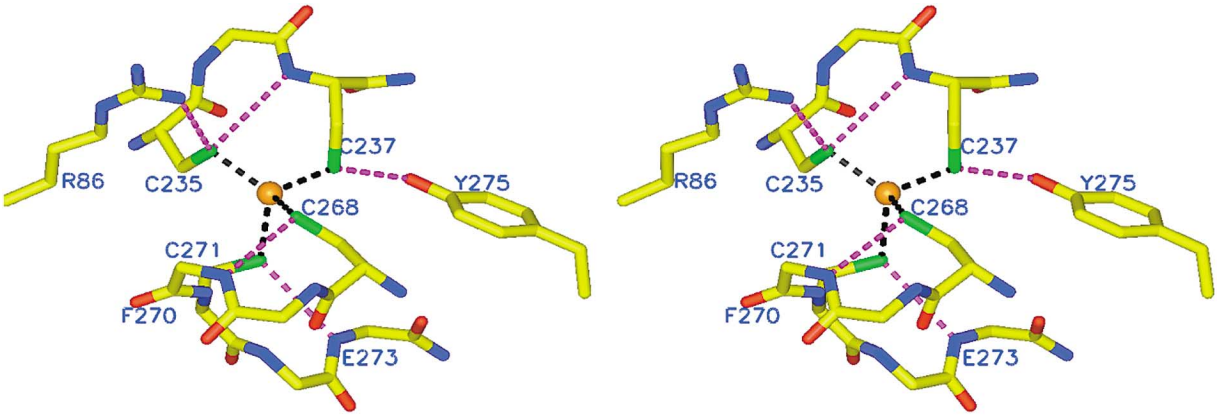

Figure 3. Stereo View of Zn^{2+} Coordination

The Zn^{2+} ion of monomer A is shown with only the side chains of the four cysteines, Arg 86, and Tyr 275 shown. Hydrogen bonds are shown as magenta lines; metal sulfur bonds are shown as black lines. Other details are in the main text.

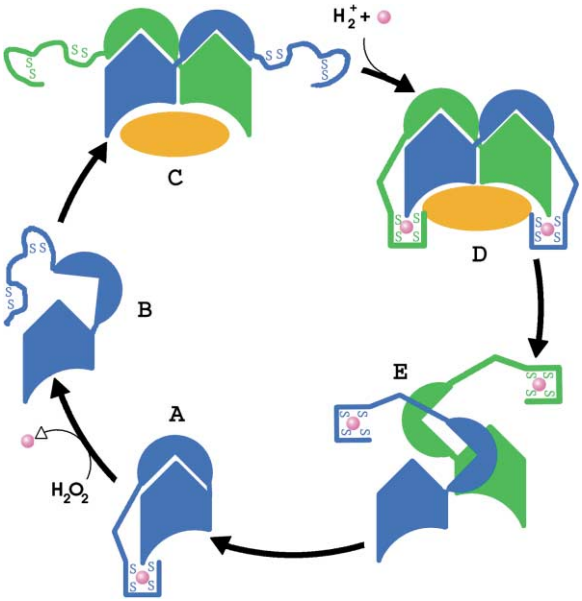

Figure 4. The Redox Regulation Cycle of Hsp33

(A) Upon exposure to oxidative stress, two disulfide bonds form in the monomeric species, and the C-terminal domain unfolds, releasing zinc (B). A high-affinity dimer is formed by domain swapping (C). Subsequent reduction allows for the formation of a kinetically stable domain-swapped dimer that coordinates zinc and retains the ability to bind protein substrates (D). Once the substrate has been released, the dimers can dissociate (E) and return to the monomeric form (A).

only fragment of the Zn^{2+} binding domain involved in this interface is the Cys-containing hairpin loop 269–271 and, notably, the side chain of Phe270, which is sequestered between Arg86 and Tyr88, stabilizing the relative orientation of the two domains. The orientation of the Zn^{2+} binding domain is also locked by the conformation of Arg86, protruding into the metal binding site from the dimerization domain. There is also an electrostatic cohesive interaction in the form of a salt bridge between Arg31 and Glu273. Overall, the total buried surface between the dimerization domain and the Zn binding domain is approximately 1000 Å^2, a mere 7% of the total solvent-accessible surface of the monomeric BsHsp33.

Molecular Mechanism of Redox Regulation of Hsp33

According to the current model, the Hsp33 proteins undergo profound structural reorganization as a result of oxidation-induced loss of Zn^{2+} and disulfide bond formation (Graf et al., 2004). The same model implies the existence of several distinct forms of the protein. The nascent form obtained under the reducing intracellular conditions is monomeric and biologically inactive. Upon exposure to an oxidative stress, two disulfides, i.e., Cys235-Cys237 and Cys268-Cys271, are formed, with concomitant loss of Zn^{2+}. Because the metal ion acts as a zipper linking two halves of the C-terminal domain, its release causes the antiparallel β hairpin to separate from the rest of the domain, which looses its tertiary structure and unfolds. This will likely result in the loss of other interdomain interactions, such as those involving Phe270.

The next step is the dimerization, a prerequisite for the chaperone activity. The two known crystal structures of the dimerization domains of the EcHsp33, which lack the presumably unfolded C-terminal domain, appear to correspond to the biologically active Hsp33 species (Kim et al., 2001; Vijayalakshmi et al., 2001), while the C-terminal Zn^{2+} binding domain of EcHsp33 (218–287) does not have any chaperone activity (S. Van Haerents and U.J., unpublished results). This indicates that the substrate binding site of Hsp33 is located in the dimerization domain. Upon reduction, the biologically active dimer does not dissociate, but maintains biological activity for some time (Hoffmann et al., 2004). These reduced, active Hsp33 dimers are further stabilized by bound protein substrate, and no significant substrate release or Hsp33 dissociation can be observed unless the DnaK-system is present. Once the substrate is released, the reduced Hsp33 dimers dissociate slowly into the inactive reduced Hsp33 monomers (Hoffmann et al., 2004). Analysis of the dissociation kinetics of substrate-free reduced Hsp33 dimers indicated that, when tested in the physiologically relevant concentration range of Hsp33 of 3–10 μM, the dissociation is a concentration-independent process, consistent with an irreversible process (Hoffmann et al., 2004).

To rationalize this cycle in structural terms, it was postulated that in the nascent, reduced Hsp33 monomer, the Zn^{2+}-bound C terminus obscures the dimerization interface and/or the functional substrate binding surfaces of Hsp33 (Graf et al., 2004). Unexpectedly, our crystal structure shows that the Zn^{2+} binding domain does not interfere with dimerization, and the protein indeed forms a homodimer similar to that postulated for the oxidized form. This would suggest that we have solved the structure of the active, reduced dimeric Hsp33 species. This, however, was somewhat surprising, given that we were able to crystallize reduced Hsp33 dimers without prior oxidation and dimerization. To assess to what extent reduced BsHsp33 monomers can indeed associate in vitro, we attempted to determine the dissociation constant (K_D) of the BsHsp33 dimer using ultracentrifugation and fluorescence anisotropy. This proved difficult due to formation of higher oligomers at high protein concentrations (>100 μM), but we were able to detect dimers of BsHsp22 down to 10 μM concentration. This is in contrast to the reduced EcHsp33, which is distinctly monomeric at these physiological concentrations (Graumann et al., 2001). This shows that the *B. subtilis* protein exhibits slightly different properties, explaining the presence of the homodimer in the crystals grown from a solution with a high protein concentration. However, upon dilution to physiologically relevant concentrations, the BsHsp33 dimers appear to quickly dissociate into the inactive monomeric species. This was confirmed with in vitro chaperone assays using both thermally unfolded and chemically unfolded substrate proteins (data not shown). We conclude that the crystal structure of the BsHsp33 corresponds to the nascent, reduced form of Hsp33, and that the dimeric state observed in the crystal is induced by the high protein concentration and may not be physiologically relevant.

What, then, are the pathways of structural changes that accompany the activation and deactivation of the chaperone function in the Hsp33 family? Figure 4 illustrates a hypothetical scheme that is consistent with our

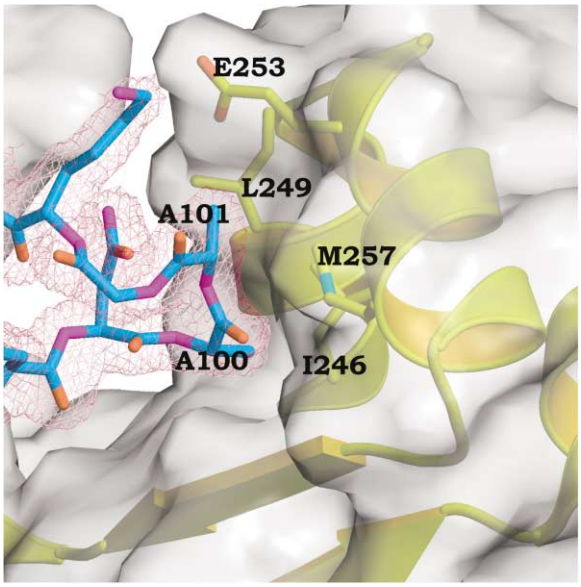

Figure 5. Crystal Contacts at Surface Mutagenesis Sites

The crystal contact mediated by the patch containing mutated sites Glu100→Ala, Gln101→Ala. A $2mF_{obs}$-DF_{calc} electron density map was contoured at 1 σ. The symmetry-related molecule is shown in ribbons representation; only selected side chains making contact with the mutated loop are shown.

structure as well as with other previous work. We suggest that the oxidation-induced unfolding of the Zn^{2+} binding domain allows for the formation of a domain-swapped, oxidized Hsp33 dimer with a much lower K_D, due to a significantly larger buried intermolecular interface. Strong experimental support for this mechanism comes from two independent crystallographic studies of the truncated EcHsp33 protein, both of which show domain swapping (Kim et al., 2001; Vijayalakshmi et al., 2001), suggesting that in the absence of the folded Zn^{2+} binding domain, this is the thermodynamically preferred species. Upon reduction and concomitant refolding of the Zn^{2+} binding domain, a domain-swapped, biologically active Zn^{2+}-bound dimer may form, as suggested by experimental studies (Hoffmann et al., 2004). However, the substrate-free reduced Hsp33 dimers are not thermodynamically stable but rather kinetically stable and dissociate slowly at 25°C. Most likely, the rate-limiting step in the dissociation process of reduced Hsp33 dimers is the formation of the nondomain-swapped Hsp33 dimer—whose structure we have solved—which can readily dissociate.

Crystal Contacts and the Surface Entropy Reduction

As stated earlier, the preparation of the X-ray quality crystals of the BsHsp33 protein was made possible by the application of the recently proposed surface entropy reduction approach (Derewenda, 2004; Garrard et al., 2001; Longenecker et al., 2001). The method relies on the concept that crystal-forming surface patches can be engineered by replacing residues with high conformational entropy (e.g., lysines, glutamates, glutamines, etc.) with residues with little or no entropy, such as alanine. A number of successful applications of this strategy have been reported to date (Janda et al., 2004; Munshi et al., 2003; Prag et al., 2003), and the method has the potential to become a routine tool. In the case of the BsHsp33 structure, the mutated residues are found on an external loop preceding helix H3 in the dimerization domain. The crystal structure shows that, in one of the monomers, this loop forms a direct contact with a symmetry-related molecule (Figure 5), although in monomer B it is not involved in crystal contacts. Nonetheless, given that the wild-type protein would not crystallize, the crystal contact mediated by molecule A was clearly critical for crystallization. The mutation site is distant from the putative functional surfaces and from the Zn^{2+} binding domain, and it is unlikely to have affected the structure of BsHsp33.

Experimental Procedures

Protein Expression and Purification

The pMCSG7 expression vector containing the *B. subtilis* Hsp33 gene with an N-terminal His_6 tag was obtained from the Midwest Center for Structural Genomics. Expression was carried out in *E. coli* BL21(DE3) strain in Luria-Bertani medium (LB). Wild-type and mutant proteins were produced after induction with 1 mM IPTG at 20°C, when OD_{600} reached 5.0. Cells were harvested by centrifugation and lysed by sonication. The soluble fractions were isolated by centrifugation, and the tagged Hsp33 protein was bound to a Ni-affinity column and subsequently eluted in an imidazole gradient (50–100 mM). Following proteolysis with rTEV, the His_6 tag was removed together with tagged protease by Ni-affinity chromatography. Hsp33 was dialyzed against a buffer containing 20 mM Tris (pH 8.0) and concentrated to 15 mg/ml (Bradford assay-BioRad).

Design and Preparation of the Crystallizable Mutant

A double mutant with a reduced surface entropy patch (Derewenda, 2004) was designed based on the existing crystal structures of the *E. coli* Hsp33 fragment (Kim et al., 2001; Vijayalakshmi et al., 2001). Two residues with high conformational entropy, Glu 100 and Gln 101, located on a solvent-exposed loop, were mutated to alanines. The mutagenesis was performed with the QuikChange kit using a single primer. The mutant was expressed and purified in the same way as the wild-type protein.

Crystallization and Data Collection

The screens using the wild-type and mutated protein were carried out using 96 solutions, a subset of the 108 best crystallization conditions reported by the Joint Center for Structural Genomics (Page et al., 2003). No crystals for the wild-type protein were observed, while the mutated protein yielded diffraction-quality crystals straight from the screen. The optimal conditions were 1.55 M K/Na tartrate, 0.1 M HEPES (pH 7.5). Because Hsp33 binds Zn^{2+}, the K/Na tartrate was gradually exchanged for 2.0 M Li_2SO_4 in 0.1 M HEPES (pH 7.5), and crystals were flash frozen in the artificial mother liquor with the addition of 20% glycerol solution as a cryoprotectant and 50 mM Zn-acetate to ensure complete saturation of the Zn binding site. Data were collected at B9X beamline at the National Synchrotron Light Source (NSLS) at nominal wavelengths of 1.28310 Å (absorption peak for Zn^{2+}) and 1.2837 Å (inflection point). The unit cell was identified as $P3_121$, $a = b = 115.3$ Å, $c = 106.4$ Å. The Matthews coefficient is 3.2 $Å^3$/Da, assuming two polypeptide chains per asymmetric unit. Processing and merging of the data was carried out with HKL2000 (Otwinowski and Minor, 1997). Further details are given in Table 1.

Structure Solution and Refinement

The anomalous substructure of two Zn^{2+} atoms was solved with SHELXD (Schneider & Sheldrick, 2002), and phases were calculated with data for both wavelengths using MLPHARE from the CCP4 suite (CCP4, 1994). Part of the model was built automatically in ARP/

wARP (Perrakis et al., 1999), which built 475 out of 582 residues expected for two full-length Hsp33 molecules in the asymmetric unit. The program O (Jones et al., 1991) was used for subsequent map interpretation and manual model building. The model was refined with REFMAC5 (Murshudov et al., 1997) against data collected at the absorption peak wavelength, with all reflections to 1.97 Å resolution. Individual isotropic displacement parameters (B factors) were used throughout. The validation of the model was carried out using MOLPROBITY (Lovell et al., 2003) and PROCHECK (Laskowski et al., 1993). Further details are given in Table 1.

Acknowledgments

We thank Dr. Frank Collart (Argonne National Laboratory) for providing the expression plasmid for the *B. subtilis* Hsp33, Aleksandra Gabrys for assistance in the early phase of this project, and Dr. Hauke Lilie for discussions. This work was supported by NIH Grant GM62615 to Z.S.D. and, in part, by NIH Grant GM065318 and a Burroughs Wellcome Fund Career Award to U.J.

Received: June 23, 2004
Revised: August 6, 2004
Accepted: August 8, 2004
Published: October 5, 2004

References

Barbirz, S., Jakob, U., and Glocker, M.O. (2000). Mass spectrometry unravels disulfide bond formation as the mechanism that activates a molecular chaperone. J. Biol. Chem. *275*, 18759–18766.

CCP4 (Collaborative Computational Project, Number 4) (1994). The CCP4 suite: programs for protein crystallography. Acta Crystallogr. D Biol. Crystallogr. *50*, 760–763.

Derewenda, Z.S. (2004). Rational protein crystallization by mutational surface engineering. Structure *12*, 529–535.

Garrard, S.M., Longenecker, K.L., Lewis, M.E., Sheffield, P.J., and Derewenda, Z.S. (2001). Expression, purification, and crystallization of the RGS-like domain from the Rho nucleotide exchange factor, PDZ-RhoGEF, using the surface entropy reduction approach. Protein Expr. Purif. *21*, 412–416.

Graf, P.C., and Jakob, U. (2002). Redox-regulated molecular chaperones. Cell. Mol. Life Sci. *59*, 1624–1631.

Graf, P.C., Martinez-Yamout, M., VanHaerents, S., Lilie, H., Dyson, J.H., and Jakob, U. (2004). Activation of the redox regulated chaperone Hsp33 by domain unfolding. J. Biol. Chem. *279*, 20529–20538.

Graumann, J., Lilie, H., Tang, X., Tucker, K.A., Hoffmann, J.H., Vijayalakshmi, J., Saper, M., Bardwell, J.C., and Jakob, U. (2001). Activation of the redox-regulated molecular chaperone Hsp33—a two-step mechanism. Structure *9*, 377–387.

Harding, M.M. (2004). The architecture of metal coordination groups in proteins. Acta Crystallogr. D Biol. Crystallogr. *60*, 849–859.

Hoffmann, J.H., Linke, K., Graf, P.C., Lilie, H., and Jakob, U. (2004). Identification of a redox-regulated chaperone network. EMBO J. *23*, 160–168.

Jakob, U., Muse, W., Eser, M., and Bardwell, J.C. (1999). Chaperone activity with a redox switch. Cell *96*, 341–352.

Jakob, U., Eser, M., and Bardwell, J.C. (2000). Redox switch of Hsp33 has a novel zinc-binding motif. J. Biol. Chem. *275*, 38302–38310.

Janda, I., Devedjiev, Y., Cooper, D., Chruszcz, M., Derewenda, U., Gabrys, A., Minor, W., Joachimiak, A., and Derewenda, Z.S. (2004). Harvesting the high-hanging fruit: the structure of the YdeN gene product from Bacillus subtilis at 1.8 A resolution. Acta Crystallogr. D Biol. Crystallogr. *60*, 1101–1107.

Jones, T.A., Zou, J.Y., Cowan, S.W., and Kjeldgaard, M. (1991). Improved methods for binding protein models in electron density maps and the location of errors in these models. Acta Crystallogr. A *47*, 110–119.

Kim, S.J., Jeong, D.G., Chi, S.W., Lee, J.S., and Ryu, S.E. (2001). Crystal structure of proteolytic fragments of the redox-sensitive Hsp33 with constitutive chaperone activity. Nat. Struct. Biol. *8*, 459–466.

Konrat, R., Weiskirchen, R., Bister, K., and Krautler, K. (1998). Bispheric coordinative structuring in a zinc finger protein: NMR analysis of a point mutant of teh carboxy-terminal LIM domain of quail cysteine- and glycine-rich protein CRP2. J. Am. Chem. Soc. *120*, 7127–7128.

Korber, P., Zander, T., Herschlag, D., and Bardwell, J.C. (1999). A new heat shock protein that binds nucleic acids. J. Biol. Chem. *274*, 249–256.

Laskowski, R.A., McArthur, M.W., Moss, D.S., and Thornton, J.M. (1993). PROCHECK: a program to check the stereochemical quality of protein structures. J. Appl. Crystallogr. *26*, 282–291.

Lesniak, J., Barton, W.A., and Nikolov, D.B. (2002). Structural and functional characterization of the Pseudomonas hydroperoxide resistance protein Ohr. EMBO J. *21*, 6649–6659.

Liu, S., Zhang, P., Ji, X., Johnson, W.W., Gilliland, G.L., and Armstrong, R.N. (1992). Contribution of tyrosine 6 to the catalytic mechanism of isoenzyme 3–3 of glutathione S-transferase. J. Biol. Chem. *267*, 4296–4299.

Longenecker, K.L., Garrard, S.M., Sheffield, P.J., and Derewenda, Z.S. (2001). Protein crystallization by rational mutagenesis of surface residues: Lys to Ala mutations promote crystallization of RhoGDI. Acta Crystallogr. D Biol. Crystallogr. *57*, 679–688.

Lovell, S.C., Davis, I.W., Arendall, W.B., III, de Bakker, P.I., Word, J.M., Prisant, M.G., Richardson, J.S., and Richardson, D.C. (2003). Structure validation by Cα geometry: phi, psi and Cβ deviation. Proteins *50*, 437–450.

Munshi, S., Hall, D.L., Kornienko, M., Darke, P.L., and Kuo, L.C. (2003). Structure of apo, unactivated insulin-like growth factor-1 receptor kinase at 1.5 A resolution. Acta Crystallogr. D Biol. Crystallogr. *59*, 1725–1730.

Murshudov, G.N., Vagin, A.A., and Dodson, E.J. (1997). Refinement of macromolecular structures by the maximum-likelihood method. Acta Crystallogr. D Biol. Crystallogr. *53*, 240–255.

Otwinowski, Z., and Minor, W. (1997). Processing of X-ray diffraction data collected in oscillation mode. Methods Enzymol. A *276*, 307–326.

Page, R., Grzechnik, S.K., Canaves, J.M., Spraggon, G., Kreusch, A., Kuhn, P., Stevens, R.C., and Lesley, S.A. (2003). Shotgun crystallization strategy for structural genomics: an optimized two-tiered crystallization screen against the Thermotoga maritima proteome. Acta Crystallogr. D Biol. Crystallogr. *59*, 1028–1037.

Perrakis, A., Morris, R., and Lamzin, V.S. (1999). Automated protein model building combined with iterative structure refinement. Nat. Struct. Biol. *6*, 458–463.

Prag, G., Misra, S., Jones, E.A., Ghirlando, R., Davies, B.A., Horazdovsky, B.F., and Hurley, J.H. (2003). Mechanism of ubiquitin recognition by the CUE domain of Vps9p. Cell *113*, 609–620.

Schneider, T.R., and Sheldrick, G.M. (2002). Substructure solution with SHELXD. Acta Crystallogr. D Biol. Crystallogr. *58*, 1772–1779.

Simonson, T., and Calimet, N. (2002). Cys(x)His(y)-Zn^{2+} interactions: thiol vs. thiolate coordination. Proteins *49*, 37–48.

Vijayalakshmi, J., Mukhergee, M.K., Graumann, J., Jakob, U., and Saper, M.A. (2001). The 2.2 Å crystal structure of Hsp33: a heat shock protein with redox-regulated chaperone activity. Structure *9*, 367–375.

Accession Numbers

The atomic coordinates were deposited in the Protein Data Bank, Research Collaboratory for Structural Bioinformatics, Rutgers University, New Brunswick, NJ, under the accession code 1vzy.pdb.